THE ASTRONOMICAL JOURNAL, 120:777–790, 2000 August

GLOBULAR CLUSTERS IN THE dE,N GALAXY NGC 3115 DW1: NEW INSIGHTS FROM SPECTROSCOPY AND *HUBBLE SPACE TELESCOPE* PHOTOMETRY

THOMAS H. PUZIA
Sternwarte der Universität Bonn, Auf dem Hügel 71, 53123 Bonn, Germany; tpuzia@astro.uni-bonn.de

MARKUS KISSLER-PATIG
European Southern Observatory, Karl-Schwarzschild-Strasse 2, 85748 Garching bei München, Germany; mkissler@eso.org

AND

JEAN P. BRODIE AND LINDA L. SCHRODER
UCO/Lick Observatory, University of California at Santa Cruz, Santa Cruz, CA 95064; brodie@ucolick.org, linda@ucolick.org
Received 2000 March 31; accepted 2000 April 27

ABSTRACT

The properties of globular clusters in dwarf galaxies are key to understanding the formation of globular cluster systems and in particular in verifying scenarios in which globular cluster systems of larger galaxies formed (at least partly) from the accretion of dwarf galaxies. Here, we revisit the globular cluster system of the dE,N galaxy NGC 3115 DW1—a companion of the nearby S0 galaxy NGC 3115—adding Keck/LRIS spectroscopy and *Hubble Space Telescope* (*HST*) Wide Field Planetary Camera 2 imaging to previous ground-based photometry. Spectra for seven globular clusters reveal normal abundance ratios with respect to the Milky Way and M31 clusters, as well as a relatively high mean metallicity ([Fe/H] $\approx -1.0 \pm 0.1$ dex). Crude kinematics indicate a high velocity dispersion within 10 kpc that could be caused either by dark matter–dominated outer regions or by the stripping of outer globular clusters by the nearby giant galaxy NGC 3115. The total galaxy mass out to 3 and 10 kpc lies between 1×10^{10} and 1×10^{11} $M_\odot$ and 2×10^{10} and 4×10^{11} $M_\odot$, respectively, depending on the mass estimator used and the assumptions on cluster orbits and systemic velocity. The *HST* imaging allows measurement of sizes for two clusters, returning core radii around 2.0 pc, similar to the sizes observed in other galaxies. Spectroscopy allows an estimate of the degree of contamination by foreground stars or background galaxies for the previous ground-based photometry but does not require a revision of previous results: NGC 3115 DW1 hosts around $N_{\rm GC} = 60 \pm 20$ clusters, which corresponds to a specific frequency of $S_{\rm N} = 4.9 \pm 1.9$, on the high end for massive dE's. Given its absolute magnitude ($M_V = -17.7$ mag) and the properties of its cluster system, NGC 3115 DW1 appears to be a transition between a luminous dE and low-luminosity E galaxy.

Key words: galaxies: individual (NGC 3115 DW1) — galaxies: kinematics and dynamics — galaxies: star clusters — globular clusters: general

1. INTRODUCTION

The study of globular cluster systems (GCSs) of dwarf galaxies complements the numerous studies of such systems in larger elliptical and spiral galaxies. Few globular cluster systems around dwarf galaxies beyond the Local Group have been studied to date with respect to their cluster system (see Ashman & Zepf 1998). This is mostly due to the low numbers of globular clusters (GCs) present in such galaxies. However, their properties are relevant for a number of globular cluster system formation scenarios. Dwarf galaxies are expected to provide insight into how the smallest galaxies build up a system of globular clusters. Further, their properties must be known in order to verify scenarios in which larger globular cluster systems are predicted to build up by the accretion of protogalactic fragments or dwarf galaxies (Kissler-Patig, Forbes, & Minniti 1998b; Côté, Marzke, & West 1998; Hilker, Infante, & Richtler 1999). These scenarios relate to the older idea that galaxy halos might have formed through the assembly of such small stellar systems (e.g., Searle & Zinn 1978).

Photometric studies of several globular cluster systems in dwarf galaxies were carried out by Durrell et al. (1996a) and Miller et al. (1998). Durrell et al. (1996a) studied the systems of 11 dwarf galaxies in the Virgo Cluster. All were found to host globular cluster candidates and have specific frequencies ranging from 3 to 8, similar to Local Group dwarfs and giant elliptical galaxies. Miller et al. (1998) studied 24 dwarf ellipticals in the Virgo and Fornax Clusters as well as in the Leo group. They found that dE,N galaxies had higher specific frequencies than dE galaxies, with values around $S_{\rm N} = 6.5 \pm 1.2$, increasing with increasing M_V (decreasing luminosity). Not much is known yet about the metallicities of globular clusters in dwarf galaxies. Minniti, Meylan, & Kissler-Patig (1996) constructed a metallicity distribution for all Local Group dwarf galaxies and noticed that the distribution was peaked around [Fe/H] ≈ -1.7 dex with no clusters more metal-rich than [Fe/H] $= -1.0$ dex. Durrell et al. (1996a) derived metallicities from Washington colors for two of their Virgo dwarf ellipticals and obtained a mean metallicity of [Fe/H] $= -1.45 \pm 0.2$ dex.

Durrell et al. (1996b) studied the GCS of the dE NGC 3115 DW1 in more detail and found it to be relatively rich (see below for a more detailed description of their results). This motivated us to carry out spectroscopy for some of the globular cluster candidates in this galaxy to get a more detailed picture of their chemical and kinematical properties. Further, *Hubble Space Telescope* (*HST*) Wide Field Planetary Camera 2 (WFPC2) data were available from the archive, allowing us to study the sizes of some of the clusters.

NGC 3115 DW1 is a dE1,N galaxy in the vicinity of the giant S0 galaxy NGC 3115. It is located at R.A. $10^{\rm h}05^{\rm m}41\overset{\rm s}{.}6$, decl. $-07°58'53''.5$ ($l = 248°.12$; $b = 36°.69$). We will assume a distance of $11^{+5.0}_{-2.3}$ Mpc throughout this paper following Durrell et al. (1996b). Additional properties will be given in the text where they are relevant. In § 2 we describe the new data. In § 3 we analyze the spectroscopic data giving first a brief kinematic study of the globular cluster system before discussing the abundances and the overall metallicity of the system. In § 4 we revisit the previous photometry (number of clusters, colors, specific frequency), compare the photometric metallicities with the spectroscopic ones, and add the *HST* WFPC2 imaging to derive sizes for two clusters. In § 5 we discuss whether NGC 3115 DW1 could have suffered stripping by its giant companion. We summarize our results in § 6.

2. DATA

2.1. *Spectroscopic Observation*

Forty-six spectra of candidate globular clusters in NGC 3115 DW1 were obtained with the LRIS-A spectrograph (Oke et al. 1995) on the Keck II Telescope during the nights of 1996 December 18 and 19. The observations were performed in multislit mode using two slit masks containing 24 (mask A) and 22 slits (mask B), respectively. Mask A was exposed for 4800 s, while mask B was exposed for 6600 s. The multiobject spectra images were taken with a Tektronix 2048×2048 pixel^2 chip. The seeing was around $0''.8$ during both nights. For all observations the first order of the 600/5000 grism (i.e., 600 lines mm^{-1}) was used with slitlets of $1''$, which provided a dispersion of 1.3 Å pixel^{-1} (at 5000 Å) and a spectral resolution of 4.1 Å FWHM^{-1}.

All frames were binned (1×2) perpendicular to the dispersion axis during the read-out. For each night the images were reduced individually and eventually combined. A master bias was created from five zero-second images, taken at the end of each night. A master flat was obtained from five twilight-flat images obtained each night. Each object image was bias-subtracted and flat-fielded in a standard way. With the IRAF[1] package APALL we traced, extracted, and sky-subtracted all object spectra. The sky was "optimally" subtracted, i.e., modeled with variance weighting perpendicular to the object spectra before being subtracted (Horne 1986). HgKrNe calibration-lamp spectra were obtained for wavelength calibration. The calibration spectra were traced, extracted, and sky-subtracted exactly in the same way as the object spectra. The wavelength calibration was verified on sky spectra included in each slit spectrum. The overall standard deviation of the wavelength calibration was determined to be $\sigma_{\rm cal} \leq 0.12$ Å for both nights.

The field of view of LRIS-A is $6' \times 8'$. We placed the multislit masks on the central/north and southeastern part of NGC 3115 DW1 as can be seen in Figure 1. The slit masks were aligned such that the slits were pointing toward the center of the giant S0 galaxy NGC 3115. Owing to the restrictions in making the masks (long enough slits, wavelength coverage, etc.), about 50% of the targets could be selected from the previous photometry of Durrell et al. (1996b; see Fig. 1). The other 50% was "blindly" selected from an LRIS acquisition image. Only six of the former group lay within $48''$ of the galaxy center, i.e., within the region where Durrell et al. (1996b) detected a clear overabundance of objects. We therefore expected about six or more objects in our total sample to be true globular clusters.

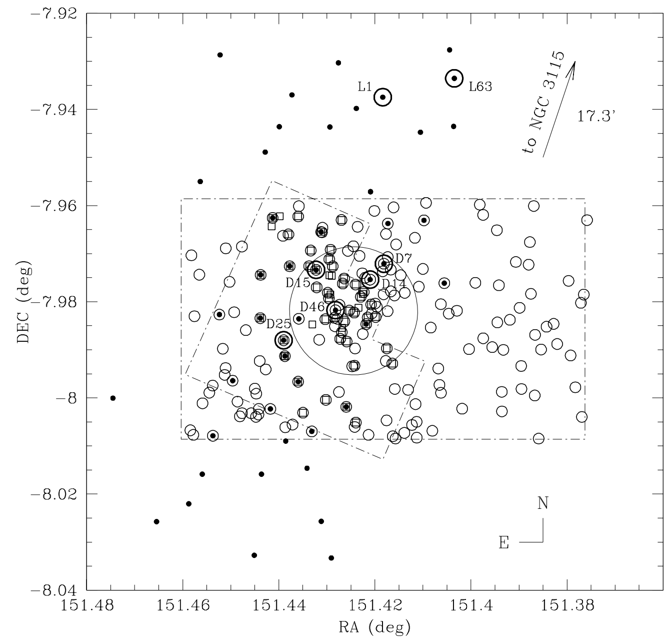

FIG. 1.—Alignment of the fields of view (FOVs) of photometry data and all spectroscopically analyzed objects around NGC 3115 DW1 is shown. Dots mark spectroscopically studied objects (this paper). Open squares are objects that were detected in a *HST* image (this paper), while open circles are objects for which photometry was obtained by Durrell et al. (1996b). Bold circles mark spectroscopically confirmed globular clusters. The dot-dashed rectangle shows the FOV of the Durrell et al. (1996b) photometry, while the dot-dashed L-shaped FOV belongs to the *HST* photometry. A large solid circle indicates the location of $r = 48''$ radius at which the object overdensity drops to background value (Durrell et al. 1996b). The distance from the center of NGC 3115 DW1 to NGC 3115 is $17'.3$ (55 kpc). The direction is indicated by the arrow in the upper right-hand corner. North is up, and east is left.

2.2. *Additional Photometry*

In order to measure sizes of globular cluster candidates that were confirmed by our spectroscopy, additional data for the globular cluster system were obtained from the *HST* archive.[2] Short exposures of 160 s in F555W and 320 s in F814W filter were taken from program GO:5999 (PI: A. Phillips). A simple reduction procedure was applied to all *HST* images: The images were biased, flat-fielded, and calibrated as described in Holtzman et al. (1995), including corrections accounting for CTE and field distortions. The brightest clusters were matched on both the F555W and F814W images, and their sizes were studied. In addition, we reanalyzed the ground-based *B*,*V* data[3] from Durrell et al. (1996b). The fields of view of both photometric data sets are overplotted in Figure 1.

[1] IRAF is distributed by the National Optical Astronomy Observatories, which are operated by the Association of Universities for Research in Astronomy, Inc., under cooperative agreement with the National Science Foundation.

[2] Based on observations made with the NASA/ESA Hubble Space Telescope, obtained from the data archive at the Space Telescope Science Institute. STScI is operated by the Association of Universities for Research in Astronomy, Inc., under NASA contract NAS 5-26555.

[3] The data were kindly provided in electronic form by Patrick Durrell.

3. ANALYSIS OF SPECTROSCOPIC DATA

In this section we extract heliocentric radial velocities v_{rad} of globular clusters and perform a mass estimate of the host galaxy, NGC 3115 DW1. Subsequently, we measure abundances using the Lick/IDS passband definitions and infer a mean metallicity of the GCS.

3.1. *Kinematics*

We derived radial velocities by two different methods. Velocities were derived by cross-correlation with high signal-to-noise ratio (S/N) template spectra of two bright GCs in M31: 225-280 and 158-213 (for nomenclature, see Huchra, Stauffer, & Van Speybroeck 1982). The cross-correlation was carried out with the IRAF task FXCOR. All measurements are summarized in Table 1. The "internal" errors that are given by the cross-correlation code lie about $\sigma \sim 80$–100 km s^{-1} for well-defined high-S/N spectra and increase rapidly as the object spectrum becomes less defined.

For seven high-S/N spectra, we also estimated the radial velocity by measuring redshifts of individual absorption lines (see footnote in Table 1). The mean radial velocity from cross-correlation served as a first guess to the mean wavelength-shift determination. We used the IRAF package RVIDLINES which employs a CENTER1D code to match the center of each individual absorption feature (see manual of RVIDLINES). We obtained an "internal" mean error from the averaging process which is ~ 100 km s^{-1}. The results and their errors are included in Table 1.

3.1.1. *Selection of Globular Clusters*

After obtaining the radial velocities from cross-correlation and in some cases from wavelength shifts of individual absorption lines, we combined all available measurements for further selection of globular clusters by radial velocity. Velocities derived from cross-correlation were given twice the weight of velocities from absorption lines. The average radial velocity for each object can be found in the second-last column of Table 1.

Figure 2 shows a radial velocity histogram of objects with $-500 \leq v_{rad} \leq 1000$ km s^{-1}. The figure shows a hint of bimodality owing to the extended tail of velocities greater than 500 km s^{-1}. Based on the measured radial velocity of NGC 3115 DW1 of ~ 700 km s^{-1} (715 ± 62 km s^{-1}, de Vaucouleurs et al. 1991; 716 ± 19 km s^{-1}, Peterson & Caldwell 1993; and 698 ± 42 km s^{-1}, Capaccioli et al. 1993) and an adopted velocity dispersion of the GCS in NGC 3115 DW1 of ~ 100 km s^{-1} (see below), globular clusters should have radial velocities in the range 400–1000 km s^{-1}. Seven candidates lie within this range. This cut enables a reliable differentiation between foreground objects of low radial velocity and globular clusters in NGC 3115 DW1.

We used the KMM code (Ashman, Bird, & Zepf 1994) to obtain the statistical significance of bimodality. The KMM code fits two Gaussians to the data using maximum likelihood techniques. The data can be fitted with two Gaussians of identical dispersion or two Gaussians of independent dispersion. We applied both techniques. The mean radial velocities of the two Gaussians are 48 ± 26 km s^{-1} and 567 ± 46 km s^{-1} for identical-dispersion and 52 ± 28 km s^{-1} and 575 ± 39 km s^{-1} for independent-dispersion fitting. The error is the error of the mean calculated from the variance of each distribution. KMM estimates also the fraction of data points that are part of each subdistribution.

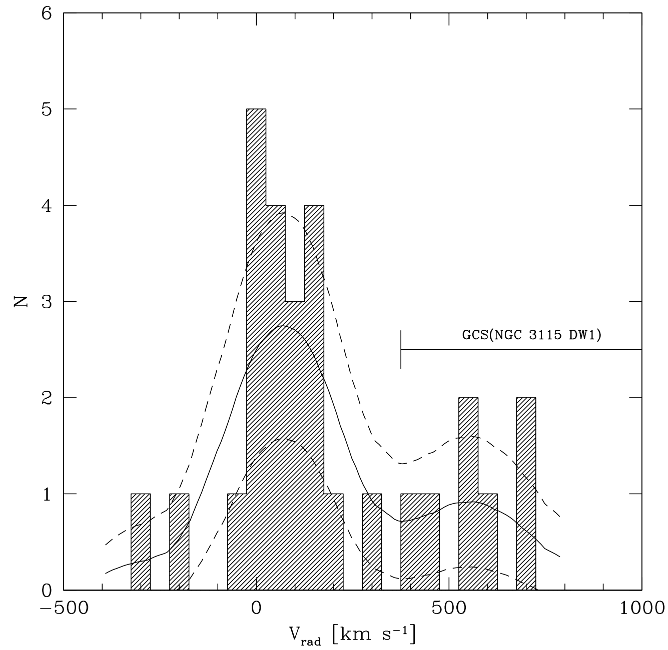

FIG. 2.—Histogram of radial velocities. Only objects with a radial velocity of $-500 \leq v_{rad} \leq 1000$ km s^{-1} have been plotted. The radial velocity range in which globular clusters are expected is indicated (object D41 with $v_{rad} = 308 \pm 45$ km s^{-1} deviates by more than 4 times the velocity dispersion of the globular cluster system from the mean system velocity of NGC 3115 DW1; it was therefore dropped). The solid line is an Epanechnikov-kernel density estimation with a kernel width of 100 km s^{-1} (for details, see Silverman 1986). Its 1 σ uncertainty is marked by the dashed lines.

Of 28 objects in the histogram (one additional object, D26, is not included owing to $v_{rad} < -500$ km s^{-1}) in Figure 2, KMM assigns 21 objects to the subpopulation with the lower mean radial velocity and seven to the subpopulation with the higher mean radial velocity, which is in good agreement with the expectations (see § 2.1). The confidence level for bimodality is greater than 99%.

The (weighted) mean radial velocity of all seven detected globular clusters is $v_{rad} = 572 \pm 30$ km s^{-1}. This value deviates from the measured radial velocity of NGC 3115 DW by $\sim 1.6\ \sigma$, which is a hint that we are biased toward lower velocities by both the small sample and the choice of slit mask position on the sky. Since we detected globular clusters predominantly in the central and northern field of NGC 3115 DW1, our measurements could be influenced by a systematic rotation of the GCS (see also § 3.1.4).

All 22 objects with low radial velocities have a weighted mean velocity of $v_{rad} = 50 \pm 19$ km s^{-1}. Assuming a simple stellar rotation model for the Milky Way, we expect the foreground stars in the direction of NGC 3115 DW1 ($l = 248^\circ.12$ and $b = 36^\circ.69$) to have $v_{rad} = 220 \sin 2l \cos^2 b = 98$ km s^{-1} (van de Kamp 1967), which is in rough agreement with our measurement.

In summary, within our data of 46 spectroscopically analyzed objects, we found seven globular clusters, 22 foreground stars, and 15 background galaxies (nine of them are significantly clumped about $v_{rad} \approx 24{,}000$ km s^{-1} or $z \approx 0.08$; the velocity dispersion of this potential galaxy cluster is $\sigma = 1300$ km s^{-1}). Two objects (D21, L6) could not be identified reliably and were therefore dropped. The radial velocity data for all objects are summarized in Table 1.

TABLE 1

RADIAL VELOCITIES FROM CROSS-CORRELATION AND INDIVIDUAL WAVELENGTH SHIFTS

Slit Number[a]	Code[b]	$V_{rad}^{158-213}$	$V_{rad}^{225-280}$	V_{rad}^{lines}	$\langle V_{rad} \rangle$	Category[c]
			Mask A			
1	L15	70,492 ± 336	70,386 ± 168	...	70,407 ± 106	⊖
2	L3	63 ± 100	81 ± 136	...	69 ± 57	*
3	L27	25,223 ± 242	25,242 ± 189	...	25,235 ± 105	⊖
4	L11	66 ± 113	105 ± 120	...	84 ± 58	*
5	L18	194 ± 74	208 ± 97	...	199 ± 42	*
6	L7	−50 ± 195	−65 ± 141	...	−60 ± 81	*
7	L16	−211 ± 178	−183 ± 162	...	−196 ± 85	*/?
8	D8	67 ± 127	101 ± 111	...	86 ± 59	*
9	D21	...	...	...	...	??
10	D10	100 ± 85	118 ± 73	...	110 ± 39	*
11	D58	1864 ± 153	23692 ± 225	...	8766 ± 89	⊖/??
12	D73	4987 ± 307	5030 ± 225	...	5015 ± 128	⊖/??
13	D20	22,542 ± 226	22,576 ± 192	...	22,562 ± 103	⊖
14	D24	160 ± 224	154 ± 223	...	157 ± 112	*
15	D14	455 ± 156	477 ± 149	478 ± 190	468 ± 71	⊕/?
16	D6	17 ± 61	32 ± 66	...	24 ± 32	*
17	D1	143 ± 73	152 ± 83	...	147 ± 39	*
18	D5	124 ± 70	139 ± 73	...	131 ± 36	*
19	L37	24,531 ± 180	24,614 ± 243	...	24,560 ± 102	⊖/??
20	L44	22,979 ± 210	23,020 ± 223	...	22,998 ± 108	⊖/??
21	L14	34 ± 111	67 ± 103	...	52 ± 53	*
22	L51	26 ± 187	71 ± 196	...	47 ± 96	*
23	L1	386 ± 76	402 ± 79	453 ± 44	420 ± 29	⊕
24	L63	545 ± 227	506 ± 222	668 ± 99	605 ± 74	⊕/?
			Mask B			
1	L8	99,434 ± 137	99,453 ± 125	...	99,444 ± 65	⊖
2	L4	55 ± 136	45 ± 109	...	49 ± 60	*
3	L6	...	...	...	...	??
4	L23	−337 ± 227	−259 ± 201	...	−293 ± 106	*/?
5	D9	9 ± 128	36 ± 117	...	24 ± 61	*
6	D36	−23 ± 152	13 ± 140	...	−4 ± 73	*
7	D26	−2599 ± 241	−2545 ± 201	...	−2567 ± 109	*/??
8	D2	−37 ± 111	24 ± 129	...	−11 ± 59	*
9	D25	540 ± 146	512 ± 158	540 ± 100	532 ± 60	⊕
10	D46	628 ± 215	619 ± 208	...	623 ± 106	⊕/??
11	D3	−22 ± 113	12 ± 112	...	−5 ± 56	*
12	D15	677 ± 67	692 ± 72	672 ± 62	681 ± 30	⊕
13	D7	685 ± 70	706 ± 74	710 ± 34	703 ± 25	⊕
14	D42	42,007 ± 264	70,422 ± 231	...	58,100 ± 123	⊖/?
15	L36	59,943 ± 215	3899 ± 176	...	26,386 ± 96	⊖/??
16	D41	262 ± 206	376 ± 224	307 ± 50	308 ± 45	*/?
17	L37	43,855 ± 162	17,383 ± 168	...	31,100 ± 82	⊖/??
18	L26	22,836 ± 339	22,952 ± 333	...	22,895 ± 168	⊖
19	L39	27,415 ± 366	22,664 ± 251	...	24,184 ± 146	⊖/??
20	L52	87 ± 287	168 ± 217	...	139 ± 122	*/??
21	L17	131,653 ± 187	131,659 ± 79	...	131,658 ± 51	⊖
22	L38	24,447 ± 135	26,512 ± 335	...	24,735 ± 89	⊖/?

NOTE.—Summary of all radial velocities including "internal" cross-correlation errors and statistical errors from line shift measurements. All radial velocities are given in km s^{-1}. V_{rad}^{lines} is a mean radial velocity calculated from redshifts of the element lines: Ca II K (3933 Å), Ca II H (3967 Å), Hδ (4101 Å), Ca I (4226 Å), Hγ (4340 Å), Fe I (4383 Å), Fe I (4528 Å), Hβ (4861 Å), Mg I (5183 Å), and Fe I (5270 Å) (Allen 1973; rest wavelengths in parentheses).

[a] Ordinal number of slits in each mask. Along the alignment of both masks slit 1 is in the most northwestern part of the field of view as shown in Fig. 1.

[b] Object identification marker. The code corresponds to markers of spectroscopically identified globular clusters in Fig. 1.

[c] Classification category of the spectrum. *, star; ⊖, galaxy; and ⊕, globular cluster. " ? " indicates that the spectrum shows only slight features of a typical spectrum in the classification category, and " ?? " indicates that because of too low S/N, no classification is possible by visual inspection.

3.1.2. *Mass Estimate of NGC 3115 DW1*

Our data sample of seven globular clusters is sufficient only for a first rough mass estimate of NGC 3115 DW1 and its M-to-L ratio. Furthermore, we rely in this section on the assumption that the system is not influenced by the nearby giant S0 galaxy, an assumption that we will question in § 5.

We used two mass estimators, which are extensively described and tested by Bahcall & Tremaine (1981) and Heisler, Tremaine, & Bahcall (1985). We applied the virial mass estimator (VME) and the projected mass estimator (PME) accounting for different orbit characteristics of the globular clusters. Since the alignment of our multislit masks is biased toward clusters of the central and northern quadrant of the galaxy, our data is subject to unknown systematic east-west rotation of the entire globular cluster system. If the angular momentum vector points along the north-south axis, we will have under- or overestimated the mass depending on the direction of rotation. Although it is possible to provide a lower mass limit from our spatially constrained cluster sample by varying the mean systemic velocity (see below), it is not possible to correct completely for the unknown total rotation of the globular cluster system (see also § 3.1.4).

We let the radial velocity of NGC 3115 DW1 (which is assumed to be the mean velocity of the GCS as well) vary over a wide range while the measured radial velocities of the globular clusters remained fixed. During each step of 10 km s^{-1} we calculated the mass of the galaxy with each mass estimator. The resulting plot (mass vs. v_{rad} of the GCS) is shown in Figure 3. Table 2 shows the lower mass limits calculated with all mass estimators.

At the highest measured radial velocity of NGC 3115 DW1 ($v_{rad} = 716 \pm 19$ km s^{-1}; Peterson & Caldwell 1993), we obtain total masses in the range (6.3×10^{10})–(3.6×10^{11}) $M_\odot$. The estimated masses for the measured mean radial velocity of the globular cluster system ($v_{rad} = 572 \pm 30$ km s^{-1}) are in the range (2.1×10^{10})–(1.0×10^{11}) $M_\odot$. The errors in Table 2 are the intrinsic, statistic, and systematic uncertainties of the mass estimate. The first is the uncertainty of the code itself (Bahcall & Tremaine 1981), while the remaining are due to the limited sample size and the uncertain distance. All masses are the total mass estimates within a galactocentric radius of $r \leq 189''.4$ or $R \leq 10.1$ kpc, respectively. This is the projected radial distance of the outermost globular cluster (L63).

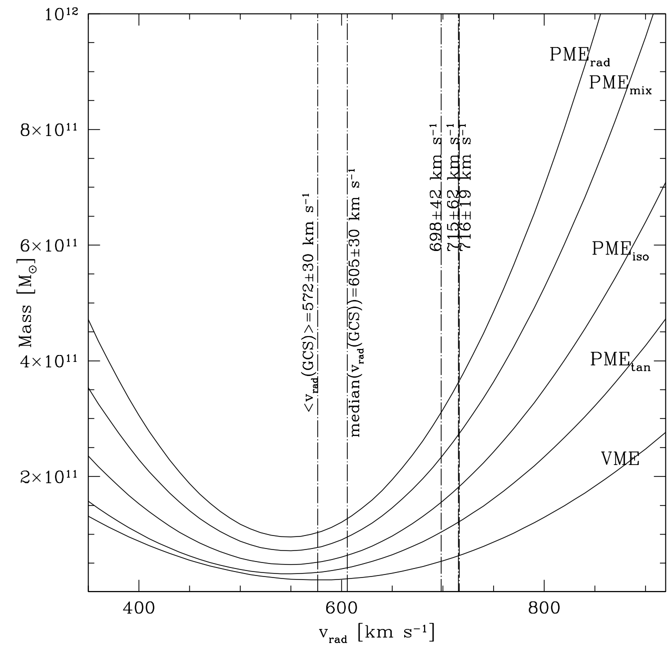

FIG. 3.—Lower mass limit estimations with two different mass estimators: PME (projected mass estimator, allowing different orbit characteristics of the GCS: rad, radial; mix, mixed; iso, isotropic; and tan, tangential orbits; see Heisler et al. 1985 for details) and VME (virial mass estimator). The measured mean radial velocity of the globular cluster system is $v_{rad} = 572 \pm 30$ km s^{-1}, while the median radial velocity was determined with $v_{rad} = 605 \pm 30$ km s^{-1}. The curves show the variation of the galaxy-mass estimate as a function of the mean system velocity. Spectroscopy of the galaxy (NGC 3115 DW1) itself gives radial velocities of 715 ± 62 km s^{-1} (de Vaucouleurs et al. 1991), 716 ± 19 km s^{-1} (Peterson & Caldwell 1993), and 698 ± 42 km s^{-1} (Capaccioli et al. 1993). The errors of each mass estimator are given in Table 2.

Assuming an *isotropic* orbit distribution for globular clusters in NGC 3115 DW1, the lower mass limit for the galaxy of $M_{PME} = (4.8 \pm 2.3) \times 10^{10}$ $M_\odot$ seems rather large for a dwarf elliptical. The absolute magnitude of $M_V = -17.7$ mag (Durrell et al. 1996b) is high as well (more than a magnitude brighter than M32, for example, and similar to NGC 4486B, although NGC 3115 DW1 has a dissimilar structure to that of these low-luminosity E galaxies). The mean absolute V magnitude for nearby dwarf ellipticals is $\langle M_V \rangle \approx -16.9$ mag (Ferguson & Binggeli 1994). Considering its mass and luminosity, we address the fact that NGC 3115 DW1 appears to be a transition-type galaxy between luminous dE's and low-luminosity ellipticals in the discussion section.

TABLE 2

LOWER MASS LIMITS OF NGC 3115 DW1

Estimator	M_{gal}	σ_{intr}[a]	σ_{stat}[b]	σ_{dist}[c]
VME	2.11	...	0.04	$^{+0.95}_{-0.45}$
PME_i	4.77	2.28	0.16	$^{+2.17}_{-1.00}$
PME_r	9.54	5.05	0.32	$^{+4.26}_{-2.00}$
PME_m	7.15	2.77	0.24	$^{+3.25}_{-1.49}$
PME_i	3.18	1.41	0.11	$^{+1.42}_{-0.67}$

NOTE.—Lower mass estimate for NGC 3115 DW1 out to a radius of $r \leq 189''.4$ or $R \leq 10.1$ kpc. All masses are given in units of 10^{10} $M_\odot$. Different orbit characteristics of the globular clusters were adopted for the mass estimate using the projected mass estimator (PME): PME_i adopts isotropic orbits, PME_r adopts radial orbits, PME_m assumes mixed, while PME_t adopts tangential globular cluster orbits (for details, see Bahcall & Tremaine 1981).

[a] Individual intrinsic uncertainty of the mass-estimation code. Note that for VME there is no analytical variance formula available.

[b] Standard uncertainty of the mass estimate due to the limited sample size as numerically determined in bootstrap tests.

[c] Systematic uncertainty due to potential distance error.

3.1.3. *Radial Dependencies and Mass-to-Light Ratios*

Limiting the data set of radial velocities to smaller radii we can probe the radial mass dependencies in NGC 3115 DW1. Clearly, statistical errors become important when we reduce the already small data set by removing the outermost globular clusters. Nonetheless, we calculate mass estimates for different radii (using the PME and assuming isotropic orbits) since the kinematics of the two outer clus-

TABLE 3

RADIAL MASS DISTRIBUTION

r_i(arcsec)	R_i (kpc)	M_i[a]	$\sigma_{\mathrm{intr},i}$[b]	$\sigma_{\mathrm{stat},i}$[c]	Number of GCs[d]
$r < 189.4$......	$R < 10.1$	4.77	2.28	0.16	7
$r < 161.4$......	$R < 8.6$	4.55	2.35	0.25	6
$r < 56.3$	$R < 3.0$	1.82	1.03	0.08	5
$r < 41.8$	$R < 2.2$	1.61	1.02	0.06	4

[a] Mass estimate for the ith projected radial distance evaluated with PME for isotropic globular cluster orbits. The masses are given in units of $10^{10}\ M_\odot$.

[b] Internal uncertainty of the mass estimation code.

[c] Standard uncertainty from bootstrap tests.

[d] Number of globular clusters included in the data sample that was used to estimate the mass at the ith radius.

ters might be influenced by the nearby giant S0. The results are summarized in Table 3.

Combining the former findings with the photometry of Durrell et al. (1996b), who found total magnitudes $V_T = 12.63 \pm 0.06$ mag and $B_T = 13.57 \pm 0.09$ mag, we estimate rough mass-to-light ratios for different radii. Applying a King profile (King 1962) with the parameters $r_c = 14\farcs4$ and $c \sim 1.4$ (Durrell et al. 1996b), we obtain at the outermost globular cluster projected radius $r = 189\farcs4$ ($R = 10.1$ kpc) $M/L_V = 52 \pm 25$ with a 1 σ uncertainty due to statistical sample size uncertainties and photometric errors. The systematic error due to distance uncertainties of NGC 3115 DW1 is $^{+67}_{-32}$. Going inward, the M-to-L_V ratio drops. At a projected radius of $r = 56\farcs3$ ($R = 3.0$ kpc) the mass-to-light ratio is $M/L_V = 22 \pm 13$.

Our analysis can be expanded by combining our results with the M/L_V measurements for the innermost part of NGC 3115 DW1. Peterson & Caldwell (1993) measure within $r \leq 3''$ (or $R \leq 160$ pc) of NGC 3115 DW1 a central velocity dispersion of $\sigma = 20$–30 km s^{-1}. They derive a M/L_V of 3 ± 2 within $r \leq 3''$. A gradient of M/L_V can therefore be traced outward from the center of the galaxy, although the uncertainties are quite large. However, all values fit well into the range given by Ferguson & Binggeli (1994) for dwarf elliptical galaxies ($M/L_V \approx 5$ for Fornax up to $M/L_V \geq 100$ for Ursa Minor).

3.1.4. *Rotation and Velocity Dispersion*

Using the maximum likelihood method of Pryor & Meylan (1993) we measure a marginal net rotation of $v_{\mathrm{rot}} = 75 \pm 70$ km s^{-1} for the globular cluster system of NGC 3115 DW1. Note that to date no dE was reported to show significant rotation of its stellar body (Ferguson & Binggeli 1994). The position angle of the rotation axis is

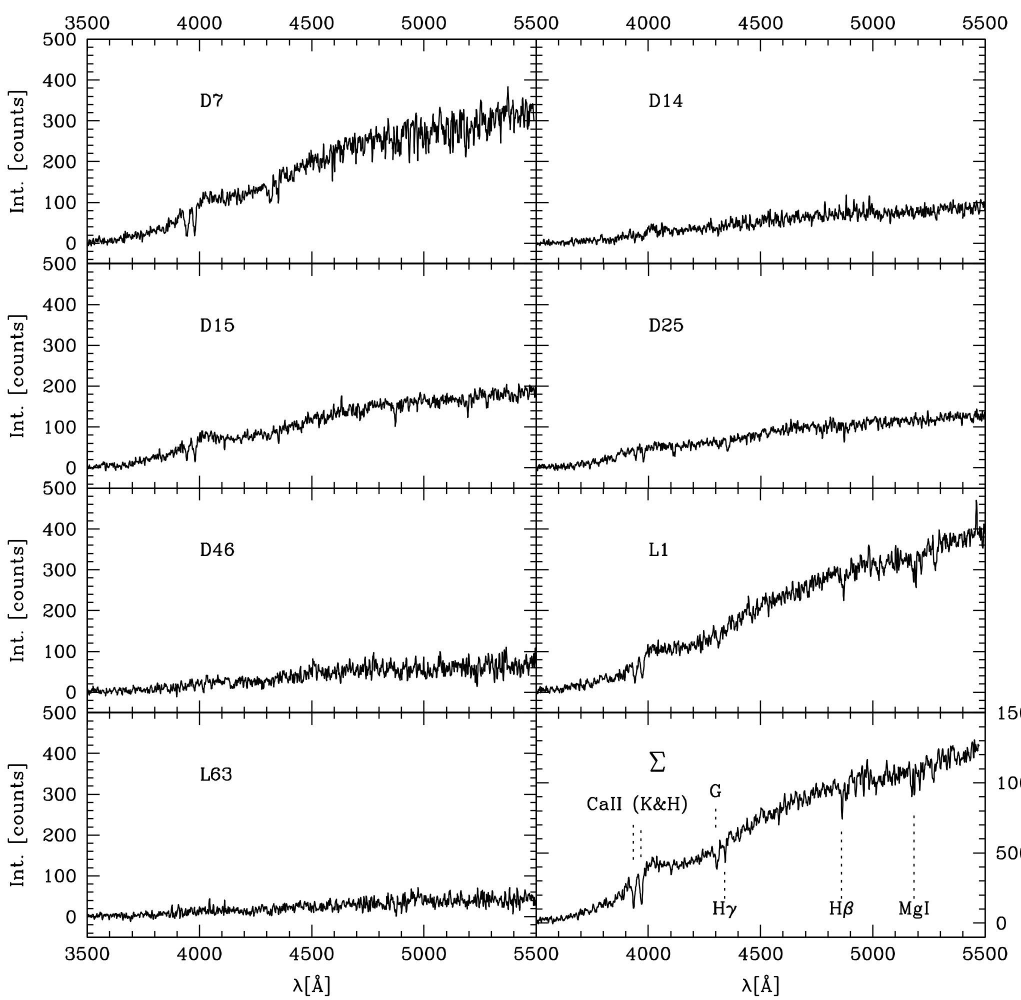

FIG. 4.—Spectra of all seven confirmed globular clusters. The S/N of the spectra ranges between 2 and 5. The bottom right-hand panel shows the combined spectrum of all other spectra. All spectra have been smoothed with a 3 pixel boxcar filter. Note the different scale of the bottom right-hand panel (combined spectrum).

TABLE 4

ABUNDANCES OF INDIVIDUAL GLOBULAR CLUSTERS AND THE ENTIRE SYSTEM

	D46			D14		
LINE/BAND	I (mag)	[Fe/H]$_i$	w_i	I (mag)	[Fe/H]$_i$	w_i
CNB	0.166 ± 0.781	−0.847	0.195	0.242 ± 0.773	−0.349	0.197
H+K	−0.152 ± 0.814	−4.430	0.155	0.459 ± 0.521	0.418	0.242
CNR	0.013 ± 0.414	−1.098	0.328	0.091 ± 0.287	−0.522	0.474
CH=G band	−0.121 ± 0.699	−3.842	0.126	0.229 ± 0.358	0.154	0.246
Hβ	0.569 ± 0.389	−0.431	...	−0.007 ± 0.215	−1.007	...
MgH	0.074 ± 0.191	−0.309	0.257	0.120 ± 0.132	0.620	0.372
MgG	0.352 ± 0.287	−0.648	...	0.041 ± 0.181	−0.959	...
Mg2	0.001 ± 0.204	−2.198	0.496	0.084 ± 0.145	−1.377	0.698
Mgb	0.185 ± 0.380	−0.815	...	0.004 ± 0.217	−0.996	...
Fe52	−0.131 ± 0.336	−4.755	0.146	0.102 ± 0.222	−0.010	0.221
⟨[Fe/H]⟩	−0.84 ± 0.82 dex			−0.86 ± 0.39 dex		

	D15			D7		
LINE/BAND	I (mag)	[Fe/H]$_i$	w_i	I (mag)	[Fe/H]$_i$	w_i
CNB	0.132 ± 0.245	−1.072	0.619	0.093 ± 0.204	−1.327	0.745
H+K	0.308 ± 0.203	−0.782	0.620	0.400 ± 0.162	−0.050	0.777
CNR	0.111 ± 0.151	−0.378	0.898	0.070 ± 0.110	−0.675	1.242
CH=G band	0.103 ± 0.178	−1.281	0.494	0.187 ± 0.116	−0.316	0.756
Hβ	−0.010 ± 0.113	−1.010	...	0.074 ± 0.079	−0.926	...
MgH	0.023 ± 0.068	−1.371	0.726	0.086 ± 0.047	−0.065	1.050
MgG	−0.040 ± 0.084	−1.040	...	−0.007 ± 0.054	−1.007	...
Mg2	0.069 ± 0.078	−1.528	1.295	0.098 ± 0.056	−1.235	1.796
Mgb	0.010 ± 0.105	−0.990	...	0.060 ± 0.066	−0.940	...
Fe52	0.080 ± 0.105	−0.461	0.467	0.090 ± 0.070	−0.245	0.701
⟨[Fe/H]⟩	−1.01 ± 0.20 dex			−0.91 ± 0.23 dex		

	D25			L1		
LINE/BAND	I (mag)	[Fe/H]$_i$	w_i	I (mag)	[Fe/H]$_i$	w_i
CNB	0.026 ± 0.363	−1.770	0.419	0.286 ± 0.178	−0.059	0.854
H+K	0.163 ± 0.316	−1.933	0.399	0.279 ± 0.159	−1.016	0.791
CNR	−0.031 ± 0.206	−1.422	0.660	0.083 ± 0.103	−0.585	1.323
CH=G band	0.105 ± 0.243	−1.259	0.363	0.057 ± 0.108	−1.805	0.818
Hβ	0.022 ± 0.185	−0.978	...	0.023 ± 0.063	−0.977	...
MgH	−0.002 ± 0.097	−1.891	0.506	0.055 ± 0.039	−0.701	1.249
MgG	−0.001 ± 0.121	−1.001	...	−0.013 ± 0.042	−1.013	...
Mg2	−0.024 ± 0.107	−2.449	0.944	0.097 ± 0.049	−1.246	2.074
Mgb	−0.041 ± 0.155	−1.041	...	−0.015 ± 0.053	−1.015	...
Fe52	0.042 ± 0.159	−1.238	0.308	0.082 ± 0.058	−0.420	0.847
⟨[Fe/H]⟩	−1.11 ± 0.37 dex			−0.98 ± 0.19 dex		

	L63			∑		
LINE/BAND	I (mag)	[Fe/H]$_i$	w_i	I (mag)	[Fe/H]$_i$	w_i
CNB	−0.603 ± 3.794	−5.903	0.040	0.123 ± 0.125	−1.133	1.215
H+K	0.022 ± 0.790	−3.048	0.159	0.274 ± 0.110	−1.052	1.147
CNR	0.237 ± 0.499	0.552	0.273	0.072 ± 0.085	−0.664	1.608
CH=G band	0.596 ± 0.634	4.347	0.139	0.128 ± 0.080	−0.999	1.104
Hβ	0.357 ± 0.445	−0.643	...	0.067 ± 0.055	−0.933	...
MgH	0.011 ± 0.220	−1.620	0.223	0.056 ± 0.035	−0.681	1.401
MgG	−0.033 ± 0.286	−1.033	...	0.008 ± 0.035	−0.992	...
Mg2	0.097 ± 0.251	−1.248	0.402	0.073 ± 0.044	−1.486	2.275
Mgb	0.235 ± 0.337	−0.765	...	0.029 ± 0.043	−0.971	...
Fe52	0.040 ± 0.336	−1.277	0.146	0.067 ± 0.051	−0.727	0.955
⟨[Fe/H]⟩	−0.81 ± 0.81 dex			−0.97 ± 0.11 dex		

NOTE.—Abundances measured with the Lick/IDS passbands defined by Brodie & Huchra 1990. The line strengths are given in mag. With the metallicity calibrations of Brodie & Huchra 1990 we derive for the ith absorption line an individual metallicity [Fe/H]$_i$. According to the statistical significance of each individual metallicity indicator its weighting w_i is given. The weighted mean metallicity of each globular cluster and of the entire GCS (indicated as ∑) is given at the bottom line. Lines which were found to be very poor or redundant metallicity indicators (Brodie & Huchra 1990) have no weighting assigned and are excluded from the averaging process. The errors include both Poisson flux uncertainties and metallicity-calibration errors.

TABLE 5

COMPARISON OF [Fe/H] FROM PHOTOMETRY AND SPECTROSCOPY

Cluster	$[Fe/H]_{spec}$	$[Fe/H]_{phot}$
D7	-0.91 ± 0.23	-0.66 ± 0.20
D14....	-0.86 ± 0.39	-0.61 ± 0.20
D15....	-1.01 ± 0.20	-1.11 ± 0.20
D25....	-1.11 ± 0.37	-1.66 ± 0.30
D46....	-0.84 ± 0.82	-1.41 ± 0.45
L1	-0.98 ± 0.19	...
L63	-0.81 ± 0.81	...
	$\langle[Fe/H]\rangle_{spec} = -0.97 \pm 0.11$	$\langle[Fe/H]\rangle_{phot} = -0.93 \pm 0.11$

NOTE.—The spectroscopical mean metallicity was obtained from the mean spectrum of seven globular clusters. Exactly the same values can be calculated by weighted averaging of individual globular cluster metallicities. The photometric mean metallicity is a weighted mean of the above values. The error of $\langle[Fe/H]\rangle_{phot}$ includes only the photometric uncertainty of the $B-V$ color. It does not include the error of the color-metallicity calibration (cf. eq. [1]).

$\theta = 90° \pm 60°$ (poorly defined given the weak rotation). This result may be of course biased by the incomplete spatial coverage of our small sample. Correcting for the net rotation we obtain a line-of-sight velocity dispersion of $\sigma = 130 \pm 15$ km s^{-1} for the full sample of seven clusters, and $\sigma = 74 \pm 36$ km s^{-1} for the inner five clusters.

The major axis of the dE1,N galaxy of $\theta_{gal} = 100° \pm 10°$ (Durrell et al. 1996b) appears at face value nearly *parallel* to the rotation axis of the GCS, although the latter is not well defined as mentioned above. Spectroscopy for more clusters with better spatial coverage is certainly needed to establish the axis alignment.

3.2. *Metallicity*

3.2.1. *Mean Metallicity of the Globular Cluster System*

The S/N values of our spectra are insufficient to establish individual cluster metallicities reliably. To measure a mean abundance for the GCS we combined all the individual spectra into a high-S/N "mean" spectrum. All individual globular cluster spectra as well as the combined spectrum are shown in Figure 4.

For abundance measurements we used the passband definitions of Brodie & Huchra (1990) and the new Lick/IDS passband definitions of Trager et al. (1998). All abundances (both of single spectra and the mean spectrum) are given in Table 4. Brodie & Huchra (1990) calibrate single element abundances with [Fe/H] using a large sample of Milky Way and M31 globular clusters. We used their calibration to estimate the mean [Fe/H] for the entire GCS, based on the composite spectrum. The mean metallicity of our globular cluster sample is $\langle[Fe/H]\rangle_{GCS} = -0.97 \pm 0.11$ dex.

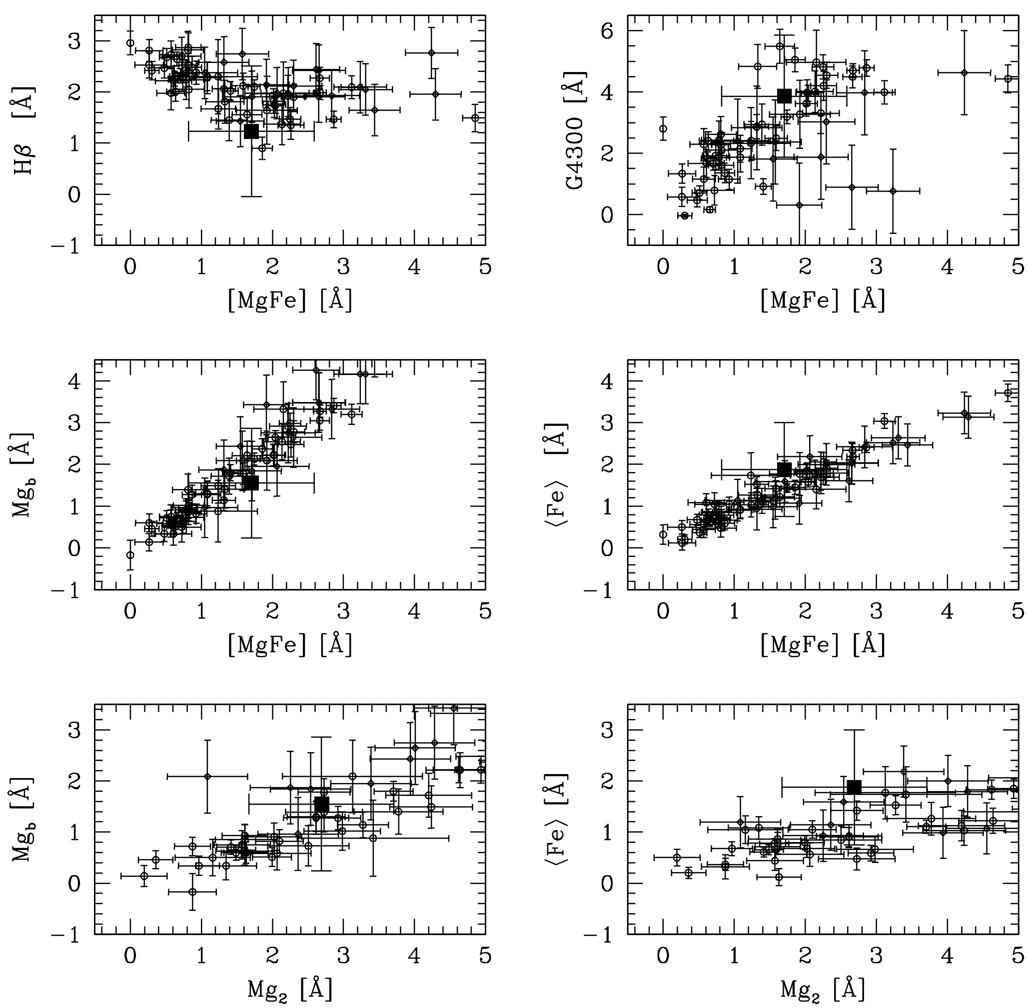

FIG. 5.—Abundance ratios of the GCS in NGC 3115 DW (*filled square*) compared to ratios of individual globular clusters in the Milky Way, M31 (*open circles*, Trager et al. 1998), and NGC 1399 (*open diamonds*, Kissler-Patig et al. 1998b). The abundances of the GCS in NGC 3115 DW1 were derived from a combined mean spectrum of seven globular clusters.

Exactly the same value is obtained from the weighted mean of the individual measurements (see Table 5).

Overall, the mean metallicity does *not* follow the empirical GCS-metallicity–galaxy-luminosity relation (see Fig. 5.7 in Ashman & Zepf 1998). NGC 3115 DW1 ($M_V = -17.7$ mag) falls in the transition region between dwarfs and elliptical galaxies, whereas the mean metallicity of the GCS falls in the range of metallicities found in giant elliptical galaxies. According to this empirical relation, NGC 3115 DW1 appears to be slightly too metal-rich for its luminosity.

3.2.2. *Abundance Ratios*

We compare the mean abundance ratios of the GCS with abundance ratios of globular clusters in other galaxies. Trager et al. (1998) provide a compilation of abundances of Milky Way and M31 globular clusters. Abundances of NGC 1399 globular clusters were measured by Kissler-Patig et al. (1998a). Both data sets use the definitions of the Lick/IDS system. In order to minimize the statistical noise of abundance measurements we calculate a mean iron abundance $\langle \mathrm{Fe} \rangle$ and a mean metal abundance [MgFe] (see González 1993 for a detailed discussion).

Figure 5 shows abundance ratios for several dominant elements. The top four panels show abundance ratios relative to the [MgFe] index. In the top left-hand panel the age-sensitive Hβ abundance is seen to be in good agreement with Milky Way and M31 data, although possibly at the lower (older) edge. The top right-hand panel shows the G band index compared with the [MgFe] index. The G band is a primary metallicity indicator (Brodie & Huchra 1990). The data show no abundance anomalies.

The two middle panels of Figure 5 could in principle be used to examine the α-element content of these globular clusters. For the stellar light of (mostly brighter) ellipticals, Worthey, Faber, & González (1992) found an α-element enhancement. The [α/Fe] enhancement is a very sensitive indicator of the star formation rate in a galaxy. As α-elements are preferentially created in Type II supernovae, their enhancement indicates a violent star formation and/or a top-heavy initial mass function (IMF). A depression, or normal values, of [α/Fe] would result from quiet star formation in which Type Ia supernovae dominate the enrichment processes. Given the relatively high mean metallicity ($\langle[\mathrm{Fe/H}]\rangle_{\mathrm{GCS}} = -0.97 \pm 0.11$ dex), a normal α-element ratio would suggest that these clusters formed from enriched material either during epochs of quiet star formation or at the very beginning of a burst. Better data could lead to interesting insights on this topic.

4. PHOTOMETRY

4.1. *Spectroscopic Check on Photometry*

The main result from the photometry of Durrell et al. (1996b) was that the GCS in NGC 3115 DW1 is rich with a specific frequency of $S_N = 4.9 \pm 1.9$ and a total globular cluster population $N_{GC} = 59 \pm 23$. Our spectroscopy and the photometric data set of Durrell et al. have 22 objects in common (see Fig. 1 and Table 6). Six of these 22 objects have projected radial distances of $r \leq 48''$ ($R \leq 2.6$ kpc). Durrell et al. consider the GCS to lie within this radius (mainly because the surface overdensity of objects disappears beyond it). We can confirm four of the six objects as bona fide globular clusters (D7, D14, D15, and D46). One object was found to be a background galaxy and another cannot be identified either by radial velocity or by its spectrum.

Assuming that this sample of six objects is a statistically representative sample of objects in the projected vicinity of NGC 3115 DW1, the upper limit of the probability of finding a globular cluster within a radius of $r \leq 48''$ ($R \leq 2.6$ kpc) around the center of NGC 3115 DW1 is $f_{GC} = 5/6 \approx 0.83$ (the lower limit is $f_{GC} = 4/6 \approx 0.67$; if we exclude the nonidentified object). This is in good agreement with the findings of Durrell et al. (1996b), although the statistical significance is very low. Durrell et al. measure the contaminating surface density of background objects to be $\sigma = 6.4 \pm 1.9$ arcmin^{-2}. Within their radial limit of $r \leq 48''$ there are a total of ~ 13 background objects. For a total population of $N_{GC} = 59 \pm 23$, the probability of picking a globular cluster within $r \leq 48''$ (and at the magnitude limit of the photometry of Durrell et al.) is $f_{GC} = 59/(13 + 59) \approx 0.82$. Our spectroscopic results suggest that there is no need to make any correction to the values for specific frequency and total globular cluster population size derived from photometry.

Miller et al. (1998) measure specific frequencies for dwarf elliptical galaxies in the Virgo and Fornax Clusters and find a log(S_N)-M_V relation for the nucleated dwarfs. NGC 3115 DW1 has a higher specific frequency ($S_N = 4.9 \pm 1.9$) than the $S_N \approx 2.2$ derived from Miller et al.'s relation for group and cluster dE,N galaxies.

Figure 6 shows the CMD of objects with $r \leq 48''$ ($R \leq 2.6$ kpc), which have been marked by open squares. Objects with photometry by Durrell et al., spectroscopically identified foreground stars, background galaxies, and globular

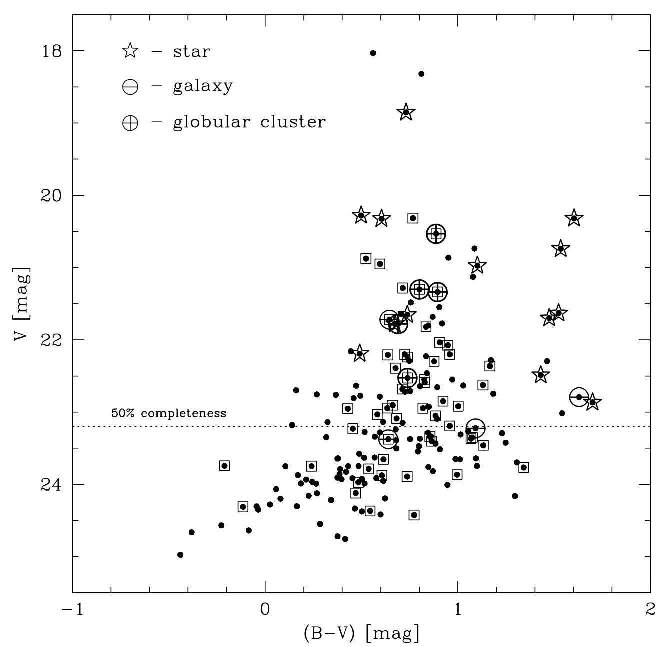

FIG. 6.—Color-magnitude diagram of objects in the vicinity of NGC 3115 DW1. Dots are objects with photometry by Durrell et al. (1996b). Open squares mark objects with $r \leq 48''$ ($R \leq 2.6$ kpc) projected distance to the galaxy center. Open stars are spectroscopically verified foreground stars, circled dashes mark background galaxies, and circled plus signs are bona fide globular clusters. There are only five spectroscopically confirmed globular clusters with B, V photometry. Two globular clusters (L1 and L63) are not covered by the field of view of the Durrell et al. (1996b) photometry (see Fig. 1). The dotted line indicates the photometric 50% completeness limit in V.

TABLE 6

Spectroscopic and Photometric Data of All Spectroscopically Studied Objects

Label	R.A. (J2000)[a] (deg)	Decl. (J2000)[a] (deg)	V[b] (mag)	$(V-I)$[c] (mag)	$(B-V)$[d] (mag)	r[e] (arcsec)	R[e] (pc)	$\langle V_{rad} \rangle$[f] (km s^{-1})
				Mask A				
L15	151.46547275	−8.02573829	...	...	...	215.2	11474	70407 ± 106
L3	151.44513389	−8.03275119	...	...	...	197.4	10525	69 ± 57
L27	151.45595107	−8.01588459	...	...	...	166.1	8856	25235 ± 105
L11	151.47453033	−8.00005692	...	...	...	190.1	10139	84 ± 58
L18	151.45373013	−8.00788268	21.65 ± 0.05	...	0.74 ± 0.06	140.2	7475	199 ± 42
L7	151.43413151	−8.01463921	...	...	...	122.8	6549	−60 ± 81
L16	151.43857103	−8.00897480	...	...	...	109.7	5850	−196 ± 85
D8	151.44176680	−8.00230439	21.70 ± 0.02	...	1.47 ± 0.06	96.0	5117	86 ± 59
D21......	151.42597410	−8.00187100	21.64 ± 0.03	1.37 ± 0.06	0.70 ± 0.04	72.1	3845	...
D10......	151.45237834	−7.98267887	20.97 ± 0.02	...	1.10 ± 0.03	99.6	5312	110 ± 39
D58......	151.43598000	−7.99663820	23.22 ± 0.11	2.09 ± 0.10	1.09 ± 0.18	67.1	3579	8766 ± 89
D73......	151.43584940	−7.98355023	23.38 ± 0.09	...	0.64 ± 0.15	41.1	2190	5015 ± 128
D20......	151.42182290	−7.98467580	21.72 ± 0.04	1.55 ± 0.15	0.65 ± 0.06	13.7	731	22562 ± 103
D24......	151.43774990	−7.97262110	21.78 ± 0.04	1.28 ± 0.07	0.67 ± 0.07	58.0	3093	157 ± 112
D14......	151.42099595	−7.97540485	21.34 ± 0.03	...	0.90 ± 0.04	26.4	1409	468 ± 71
D6	151.43119970	−7.96549650	20.28 ± 0.02	1.58 ± 0.03	0.50 ± 0.03	63.8	3401	24 ± 32
D1	151.40556550	−7.97613822	18.85 ± 0.01	...	0.73 ± 0.01	70.5	3757	147 ± 39
D5	151.41731295	−7.96373779	20.32 ± 0.01	...	0.60 ± 0.02	70.2	3742	131 ± 36
L37	151.42092628	−7.95714247	...	...	...	90.0	4800	24560 ± 102
L44	151.43991405	−7.94358566	...	...	...	148.5	7922	22998 ± 108
L14	151.43728995	−7.93698967	...	...	...	168.0	8961	52 ± 53
L51	151.42385948	−7.93980723	...	...	...	151.5	8082	47 ± 96
L1	151.41836728	−7.93746430	...	...	...	161.4	8609	420 ± 29
L63	151.40348832	−7.93354949	...	...	...	189.4	10102	605 ± 74
				Mask B				
L8	151.42908177	−8.03330443	...	...	...	185.8	9908	99444 ± 65
L4	151.45874258	−8.02204502	...	...	...	189.3	10095	49 ± 60
L6	151.43119125	−8.02568813	...	...	...	159.5	8504	...
L23	151.44361588	−8.01586187	...	...	...	140.1	7469	−293 ± 106
D9	151.43313299	−8.00698070	21.63 ± 0.02	...	1.52 ± 0.06	95.5	5090	24 ± 61
D36......	151.44962050	−7.99643065	22.86 ± 0.07	...	1.70 ± 0.17	103.9	5539	−4 ± 73
D26......	151.44384880	−7.98342710	22.49 ± 0.07	1.25 ± 0.11	1.43 ± 0.13	69.4	3700	−2567 ± 109
D2	151.43874410	−7.99131620	20.32 ± 0.02	2.69 ± 0.04	1.60 ± 0.03	61.2	3264	−11 ± 59
D25......	151.43899620	−7.98802330	21.78 ± 0.04	1.27 ± 0.07	0.69 ± 0.06	56.3	3005	532 ± 60
D46......	151.42821583	−7.98176333	22.53 ± 0.05	...	0.74 ± 0.09	13.4	716	623 ± 106
D3	151.44378760	−7.97441980	20.74 ± 0.02	3.32 ± 0.03	1.53 ± 0.04	74.0	3947	−5 ± 56
D15......	151.43225130	−7.97337860	21.30 ± 0.02	1.52 ± 0.05	0.80 ± 0.04	41.4	2208	681 ± 30
D7	151.41813758	−7.97210601	20.53 ± 0.03	...	0.89 ± 0.04	41.8	2231	703 ± 25
D42......	151.44129540	−7.96256740	22.79 ± 0.07	1.56 ± 0.10	1.63 ± 0.18	91.9	4902	58100 ± 123
L36	151.45635892	−7.95500702	...	...	...	149.4	7966	26386 ± 96
D41......	151.40979676	−7.96307913	22.19 ± 0.04	...	0.49 ± 0.06	85.6	4563	308 ± 45
L37	151.42092628	−7.95714247	...	...	...	90.0	4800	31100 ± 82
L26	151.44282349	−7.94889087	...	...	...	135.7	7236	22895 ± 168
L39	151.42936599	−7.94366459	...	...	...	138.8	7400	24184 ± 146
L52	151.41051686	−7.94476283	...	...	...	142.6	7606	139 ± 122
L17	151.45223278	−7.92867126	...	...	...	215.7	11504	131658 ± 51
L38	151.42761022	−7.93031858	...	...	...	186.0	9921	24735 ± 89

[a] Both R.A. and decl. have an accuracy of δ(R.A., decl.) $\leq 2''$. The center of NGC 3115 DW1 has the coordinates R.A. = 151.4232917 and decl. = 7.981527778.

[b] All V magnitudes were taken from Durrell et al. 1996b.

[c] V in $V-I$ was obtained from Durrell et al. 1996b, while the I magnitude was taken from our *HST* photometry. Note that the $V-I$ color suffers large uncertainty because of low S/N of the F814W images. The $V-I$ color is not corrected for galactic extinction and has to be dereddened ($E_{B-V} = 0.052$ mag [Schlegel et al. 1998]; $E_{V-I} = 1.3 \times E_{B-V}$ [Dean, Warren, & Cousins 1978] yields $E_{V-I} = 0.068$ mag).

[d] $B-V$ was obtained from Durrell et al. 1996b.

[e] Projected radial distance to the center of NGC 3115 DW1.

[f] Mean radial velocity calculated from cross-correlations and line shifts.

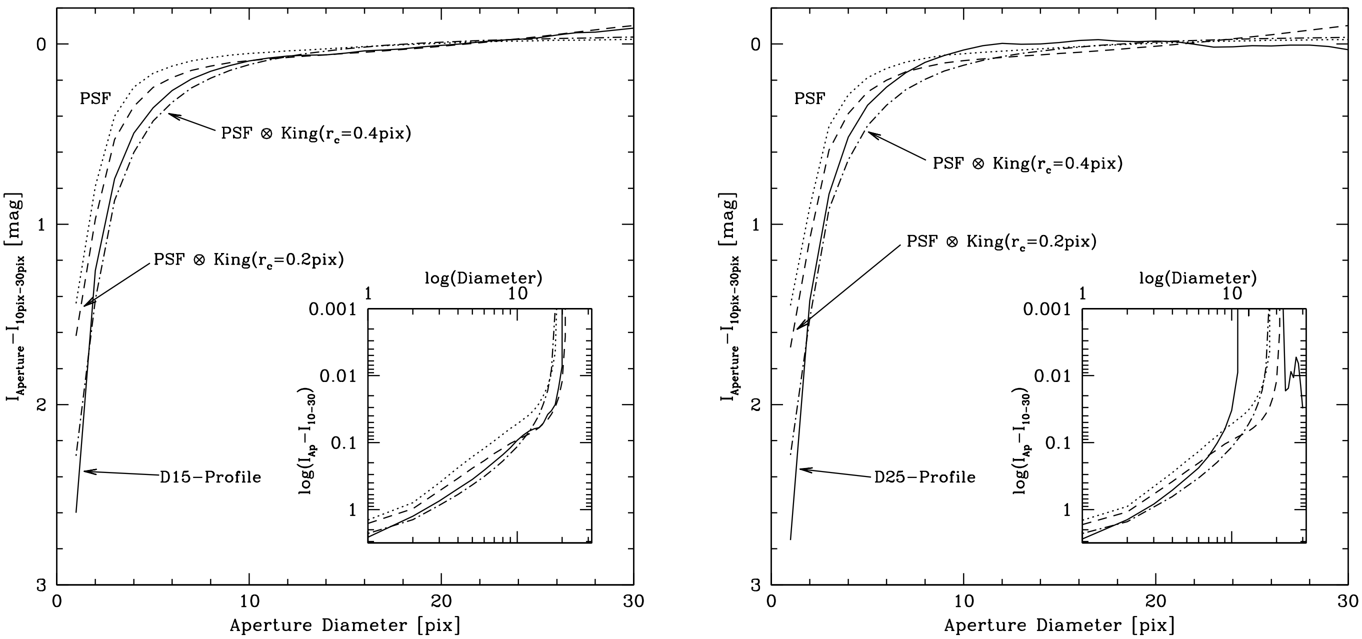

FIG. 7.—Radial intensity profiles for globular cluster D15 (*left*) and D25 (*right*). Two synthetic profiles are shown, which were created by a convolution of two King profiles with core radii $r = 0.2$ pixel ($R = 0.5$ pc, *dashed curve*) and $r = 0.4$ pixel ($R = 1.0$ pc, *dot-dashed curve*) and the corresponding *HST* PSF. Also shown is a point-source *HST* PSF (*dotted curve*). The inlays show the same curves in log-log scale.

clusters are indicated. We determined the mean color of five globular clusters (two spectroscopically confirmed globular clusters are not included in the photometric sample) in this CMD with maximum likelihood techniques. We obtained $\langle(B-V)\rangle_{GCS} = 0.82 \pm 0.04$ mag with a dispersion of $\sigma(B-V)_{GCS} = 0.06 \pm 0.04$ mag. Durrell et al. found $\langle(B-V)\rangle = 0.74 \pm 0.03$ mag, $\sigma(B-V) = 0.13$ mag for the total sample, i.e., corresponding to a lower mean metallicity. Our subset seems to be slightly biased toward metal-rich objects.

4.2. *Comparison of Photometrically and Spectroscopically Derived Metallicities*

In order to constrain the significance of photometrically derived metallicities, we transform the $B-V$ color into a [Fe/H] metallicity and compare it with the findings of our abundance measurements. For this purpose we use the relation of Couture, Harris, & Allwright (1990),

$$[\mathrm{Fe/H}] = 5.0 \times (B - V)_{\circ} - 4.86 \ , \qquad (1)$$

with [Fe/H] being the independent parameter during the calibration of the equation. The application of equation (1) to all dereddened ($E_{B-V} = 0.052$ mag; Schlegel, Finkbeiner, & Davis 1998) globular cluster colors in our NGC 3115 DW1 sample leads to photometrically derived metallicities which can be compared with the [Fe/H] values from spectroscopy. All data are summarized in Table 5. The resulting weighted mean metallicity is $\langle[\mathrm{Fe/H}]\rangle_{GCS} = -0.93 \pm 0.11$ dex (for the five globular clusters) with a dispersion of $\sigma([\mathrm{Fe/H}])_{GCS} = 0.41 \pm 0.20$ dex, in good agreement with the values derived from spectroscopy. The uncertainty results from the photometric error of the color only. No transformation uncertainty was included.

4.3. *Globular Cluster Sizes*

We matched two spectroscopically confirmed globular clusters, D15 and D25 (see Fig. 1 and Table 6), in the *HST* images taken from the archive (both on WF chips). At the distance of NGC 3115 DW1, the WF chips resolve globular clusters with core radii of $r_c \sim 5$ pc. Only 14% of Milky Way globular clusters show core radii larger than 5 pc (Harris 1999).[4] However, we can use the *HST* data to derive upper limits for the globular cluster sizes. Only images taken through the F814W filter were used because of their higher S/N.

The radial source profile $I(r)$ (i.e., the PSF of the final image) is a convolution of the object profile $O(r)$ with the telescope PSF $T(r)$ and an additive noise term $R(r)$ (r being the radial distance from the center of the profile):

$$I(r) = \int_{r_{\min}}^{r_{\max}} O(s)T(r, s)ds + R(r) \ . \qquad (2)$$

To calculate the telescope PSF profile $T(r)$ we used the TinyTim version 4.4 code by Krist & Hook (1997),[5] which gives a semianalytic estimation of the *HST* PSF for each chip, each chip position, and each filter. We adopted a King profile (King 1962) for $O(r)$, which appears to be a good fit to globular cluster radial profiles in Milky Way (e.g., Trager, King, & Djorgovski 1995) and extragalactic systems (Grillmair et al. 1996 in M31, Elson & Freeman 1985 in LMC, Kundu & Whitmore 1998 in NGC 3115, Kundu et al. 1999 in M87, and Puzia et al. 1999 in NGC 4472). From an analysis of Milky Way globular clusters (Harris 1999) we chose $c \equiv \log(r_t/r_c) = 1.5$ as a concentration parameter.

In equation (2) we neglect the additive noise term since our size estimation errors are dominated by the convolution of the poorly defined charge-diffusion matrix with the optical *HST* PSF (see Krist & Hook 1997 for a detailed discussion). Note that the charge-diffusion smears 25% of the infalling light of the central pixel among its neighbors. For consistency with other work, we continue to use this

[4] Catalog of Parameters for Milky Way Globular Clusters available at http://physun.physics.mcmaster.ca/Globular.html.

[5] Available at http://scivax.stsci.edu/krist/tinytim.html.

convolution throughout our analysis despite the fact that the diffusion correction has been derived only for the F555W filter and is thought to be wavelength dependent.

Five King profiles were generated with core radii in the range $r_c = 0.1$–0.5 pixels ($R_c = 0.5$–2.7 pc). In addition, we generated *HST* PSFs for both our identified globular clusters using individual specifications (e.g., filter, chip, chip position). Both *HST* PSFs were convolved with all the King profiles. Aperture photometry was applied to all generated profiles and both globular clusters on the *HST* images. For this purpose we used SExtractor (Bertin & Arnouts 1996) and measured magnitudes in 30 apertures with diameters in the range 1–30 pixels. All magnitudes were normalized to the average aperture magnitudes in the range 10–30 pixels, i.e., $I(r) = I_o(r) - \langle I \rangle_{10-30 \text{ pixels}}$. Figure 7 shows the profiles of both globular clusters, a raw *HST* PSF profile, and two of the convolution profiles with core radii of $r_c = 0.2$ and 0.4 pixels.

Both globular cluster profiles deviate significantly from the raw *HST* PSF profile, which indicates that both D15 and D25 are resolved. The S/N of the F814W image drops to 1 at an aperture diameter of 6 pixels. For larger apertures, there is insufficient signal to detect any deviations from a raw *HST* PSF. For smaller apertures both globular cluster profiles lie between King profiles of core radii 0.2 and 0.4 pixels. We deduce an upper limit for both globular cluster sizes of $r_c = 2.1^{+0.9}_{-0.4}$ pc at an adopted distance of NGC 3115 DW1 of $d = 11^{+5.0}_{-2.3}$ Mpc (Durrell et al. 1996b). Twenty-seven percent of Milky Way globular clusters have core radii larger than 2.1 pc (Harris 1999), and 10% have sizes in the range defined by the errors of the NGC 3115 DW1 clusters.

This upper limit compares well with the results of Kundu & Whitmore (1998) and Kundu et al. (1999). Using *HST* photometry, these authors find typical half-light radii[6] of $r_h = 2.0 \pm 0.1$ pc and $r_h \approx 2.5$ pc for globular clusters in NGC 3115 and M87, respectively.

5. DISCUSSION

In § 3.1.4, we derived a high globular cluster velocity dispersion, and thus a high galaxy mass, when we included the two outermost globular clusters. The high mass is not unexpected given the bright absolute magnitude of NGC 3115 DW1. Based on its $M_B = -16.8$ mag (Durrell et al. 1996b), NGC 3115 DW1 falls in the transition region between dwarfs and ellipticals in the mass-luminosity relation of Dekel & Silk (1986, see Fig. 3 therein). Its high mass $[M_{\rm PME} = (4.8 \pm 2.3) \times 10^{10}\ M_\odot]$ and the high velocity dispersion ($\sigma = 130 \pm 15$ km s^{-1}; see below) are more consistent with an elliptical galaxy. We therefore discuss whether the two outermost clusters could be in the process of being stripped by the nearby giant S0 galaxy NGC 3115.

5.1. *Possible Stripping?*

Figure 1 and Table 6 show that two (L1 and L63) of the seven globular clusters have significantly larger projected radii, i.e., 161''.4 (8.6 kpc, L1) and 189''.4 (10.1 kpc, L63), than the "inner" ($r \leq 56''.3 = 3$ kpc) globular clusters. These large projected distances from NGC 3115 DW1 could be due to stripping by the nearby S0 galaxy NGC 3115. Figure 8 shows the relative positions of NGC 3115 DW1 and NGC 3115. The projected distance between the two galaxies is 17'.3, which corresponds to 55 kpc at the distance of $d \approx 11$ Mpc. The mean radial velocities of L1 and L63 are $v_{\rm rad} = 420 \pm 29$ km s^{-1} and $v_{\rm rad} = 605 \pm 74$ km s^{-1}, respectively. Only L1 shows a significant deviation from the systemic velocity of NGC 3115 DW1 ($v_{\rm rad} = 698 \pm 74$ km s^{-1}; Capaccioli et al. 1993) and NGC 3115 ($v_{\rm rad} = 663 \pm 6$ km s^{-1}; Capaccioli et al. 1993).

We expect no contamination from globular clusters of the nearby galaxy NGC 3115. Kavelaars (1997) found the surface density overabundance of globular clusters around NGC 3115 (power-law index of radial distribution $\alpha = -1.8 \pm 0.5$) disappearing at 6' radius from the center of NGC 3115 (at a photometric limit of $V = 23.5$ mag). The globular clusters L1 and L63 have a radial distance to NGC 3115 of $\approx 14'$. The projected GC surface density of the GCS of NGC 3115 at the position of these two clusters is less than 0.01 arcmin^{-2}. The extrapolated GC surface density of NGC 3115 DW1 at this position lies between 0.2 and 6.9 GCs arcmin^{-2}, given the large uncertainties on the density profile. As the numbers are too small (we found only two clusters to the north and none to the south), it cannot statistically be concluded whether the two globular clusters found in the northern field are chance detections or a statistically significant overabundance.

Assuming that both galaxies are roughly at the same distance, we can estimate the dwarf galaxy's gravitational potential and the ratio of potentials of NGC 3115 DW1 and NGC 3115. Both globular clusters are at about one-fifth of the distance separating NGC 3115 DW1 and NGC 3115. As a rough estimate, we assume that NGC 3115 DW1 and NGC 3115 have similar M/L_V. In this case, the ratio of their M_V's would imply that NGC 3115 has a mass 10 times larger than NGC 3115 DW1. Hence, the gravitational potentials are comparable at the projected position of the distant globular clusters (L1 and L63). Because the mass of NGC 3115 is likely to be higher than the adopted value (assuming an extended dark matter halo), the motion of both globular clusters is no longer dominated by the gravitational potential of NGC 3115 DW1 alone. Both clusters could then be considered as intergalactic globular clusters.

Note that stripping of globular clusters appears to be common among interacting galaxies. Da Costa & Armandroff (1995) show that four globular clusters of the Sagittarius dSph are in the process of being stripped by the Milky Way and are being added to its globular cluster system. Other studies have indicated that stripping may be important in galaxy clusters (e.g., in the Fornax Cluster—Kissler-Patig et al. 1999; Hilker, Infante, & Richtler 1999). However, there are no other (optical) hints of interaction from NGC 3115 DW1's stellar light. Durrell et al. (1996b) found the isophotes to be consistent with little or no tidal disruption out to a projected radius of 60'' (corresponding to 3.2 kpc) where their photometric errors start to dominate.

A simple test for the stripping hypothesis would be a wide-field study of the system in order to rule out (spectroscopically) the presence of any similar clusters around NGC 3115 DW1.

5.2. *The Expected Velocity Dispersion*

A look at the fundamental plane of dwarf elliptical galaxies (e.g., Peterson & Caldwell 1993) shows that NGC

[6] The half-light radius is comparable with the core radius of a King profile.

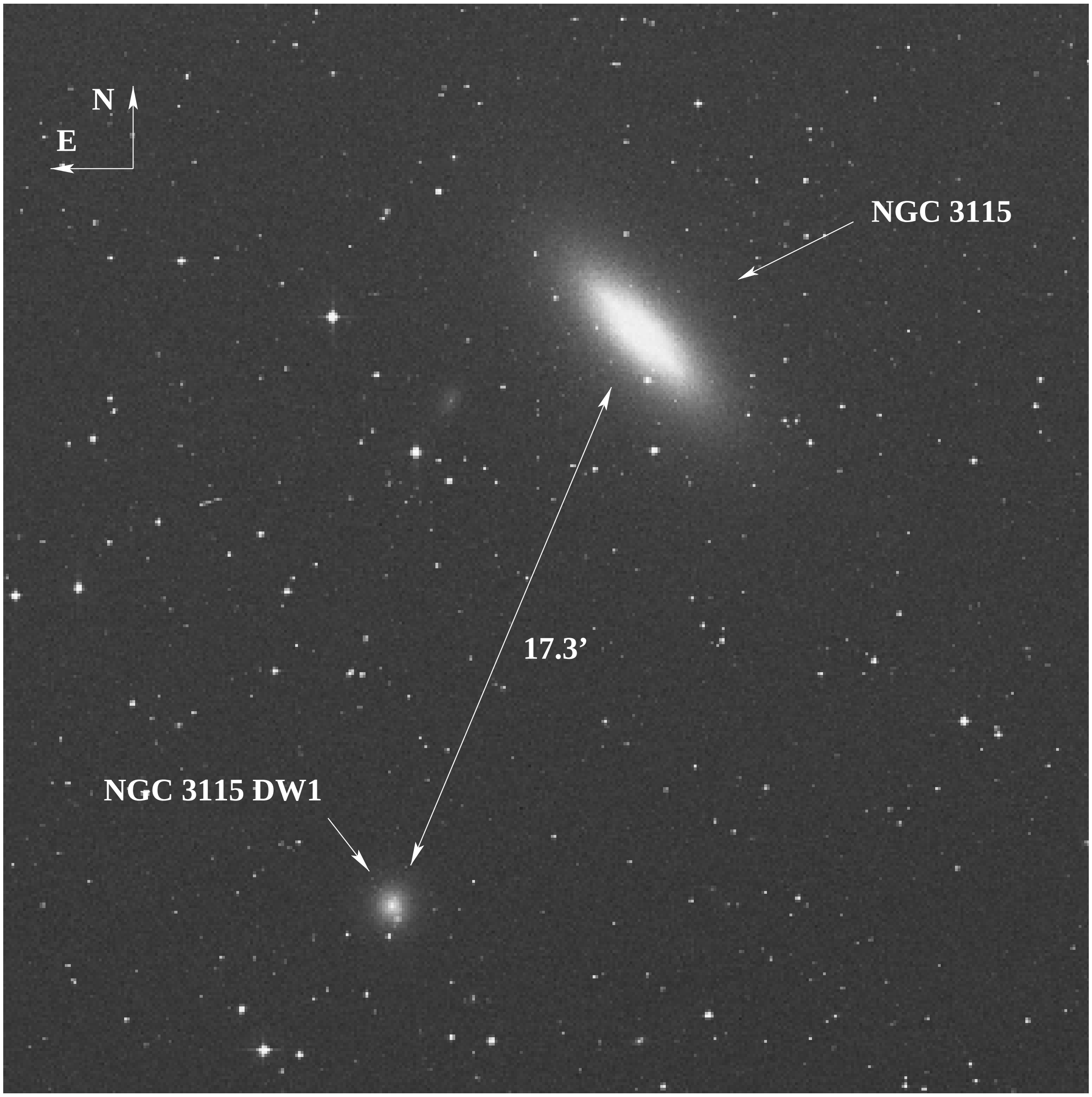

FIG. 8.—Relative positions of the dwarf elliptical galaxy NGC 3115 DW1 and the S0 galaxy NGC 3115. The projected distance between these two galaxies is 17$'$.3 (55 kpc). The image was taken from the Digitized Sky Survey. The size is 30$'$ × 30$'$.

3115 DW1 fits reasonably well into the relation for dwarf and giant elliptical galaxies, under their assumption of $M_V = -16.7$ mag. Adopting the absolute magnitude of $M_V = -17.7$ mag (Durrell et al. 1996a), the galaxy falls slightly off the relation and would imply a higher velocity dispersion than measured in the central 3$''$. With the measured velocity dispersion of $\sigma = 74 \pm 36$ km s^{-1} for the five globular clusters inside $r < 56''.3$ ($R < 3$ kpc), we obtain from the fundamental-plane relation of Peterson & Caldwell (1993) an absolute magnitude of $M_V = -18.0 \pm 0.5$ mag. The measured velocity dispersion for the total sample of seven clusters inside $r < 189''.4$ ($R < 10.1$ kpc) of $\sigma = 130 \pm 15$ km s^{-1} would correspond to far brighter absolute magnitude ($M_V = -19.5 \pm 0.5$ mag) than the measured $M_V = -17.7$ mag. This discrepancy can be explained by a close encounter and subsequent stripping of the dwarf galaxy's halo by the nearby S0 galaxy NGC 3115. Stripping of outer halo regions might well have introduced violent perturbations and led to an enhanced velocity dispersion of the halo region (which is traced by the globular clusters). The relaxation time of such a system far exceeds the Hubble time (Binney & Tremaine 1994), and therefore it is not possible to reject this scenario just from considerations of dynamical timescales.

Alternatively, a high velocity dispersion in the outskirts of a galaxy could be due to a dark matter–dominated massive halo. The outer parts of a number of lower luminosity Local Group galaxies are known to be dominated by dark matter (e.g., Mateo 1998). This picture could explain the fact that we measure an uncommonly high mass for a dwarf elliptical (see § 3.1.2) at a projected radius of 189$''$.4 (10.1 kpc).

We cannot discriminate between the above possibilities at this point.

6. SUMMARY

Using LRIS multislit spectra we confirm, on the basis of their radial velocities, seven of the 46 objects in our spectroscopic sample as bona fide globular clusters associated with the bright ($M_V = -17.7$ mag) dE1,N galaxy, NGC 3115 DW1.

We verify the findings of Durrell et al. (1996b) (within a projected radius of $r \leq 48''$ corresponding to $R \leq 2.6$ kpc) who derived the specific frequency $S_N = 4.9 \pm 1.9$ and a total globular cluster population size $N_{GC} = 59 \pm 23$. The spectroscopic verification of foreground and background contamination indicates that no revision of these results is necessary. NGC 3115 DW1 remains a dE,N galaxy with a somewhat high S_N value.

A mass estimate using the projected mass estimator for isotropic globular cluster orbits yields a total galaxy mass of $M_{gal} = (4.8 \pm 2.3) \times 10^{10}$ $M_\odot$ (with the error being the internal uncertainty of the mass estimation code) inside a radius $r \leq 189''.4$ ($R \leq 10.1$ kpc) and $M_{gal} = (1.8 \pm 1.0) \times 10^{10}$ $M_\odot$ inside $r \leq 56''.3$ ($R \leq 3.0$ kpc). This estimate is a lower mass limit (see § 3.1.2) and assumes that the outer globular clusters are not influenced by the nearby giant S0 NGC 3115. Using two mass estimators (i.e., PME and VME; see § 3.1.2) and various assumptions for the systemic velocity and the cluster orbits, we derive masses between 2×10^{10} and 4×10^{11} $M_\odot$. The mass increases with radius (see Table 3). Inside $R < 160$ pc, the mass-to-light ratio was found to be $M/L_V = 3 \pm 2$ (Peterson & Caldwell 1993) and increases with radius, leading to $M/L_V = 52 \pm 25$ at ~ 10 kpc (using the PME and assuming isotropic orbits), compatible with dark matter–dominated outer regions. However, we cannot at present exclude the possibility that the high velocity dispersion is due to stripping of the two outer clusters by the nearby giant companion.

A kinematic analysis shows that the globular cluster system has a marginal net rotation of $v_{rot} = 75 \pm 70$ km s^{-1} with a position angle of the rotation axis $\theta = 90° \pm 60°$. Subtracting the net rotation we find a line-of-sight velocity dispersion of the globular cluster system of $\sigma = 130 \pm 15$ km s^{-1} for the total sample of seven globular clusters and $\sigma = 74 \pm 36$ km s^{-1} for the inner five clusters (see § 3.1.4).

We measure mean abundances (using Lick/IDS passband definitions) from a combined mean spectrum of all seven globular clusters and derive a mean GCS metallicity of $\langle[\mathrm{Fe/H}]\rangle_{GCS} = -0.97 \pm 0.11$ dex. All abundance ratios appear similar to the ones measured in Milky Way, M31, and NGC 1399 globular clusters.

The mean color of the spectroscopically confirmed globular clusters is $\langle(B-V)\rangle_{GCS} = 0.82 \pm 0.04$ mag with a dispersion $\sigma(B-V)_{GCS} = 0.06 \pm 0.04$ mag.

Applying the color-metallicity calibration of Couture et al. (1990) we obtain a photometric mean metallicity $\langle[\mathrm{Fe/H}]\rangle_{GCS} = -0.93 \pm 0.11$ dex with a dispersion of $\sigma([\mathrm{Fe/H}])_{GCS} = 0.41 \pm 0.20$ dex (the error being the photometric uncertainty).

For two globular clusters (L1 and L63) with *HST* photometry, we derive upper limits for their core radii. These were found to be $r_c = 2.1^{+0.9}_{-0.4}$ pc.

We would like to thank Patrick Durrell for providing his ground-based photometry in electronic form. We also thank Duncan Forbes for his help during the observation.

Some of the data presented herein were obtained at the W. M. Keck Observatory, which is operated as a scientific partnership among the California Institute of Technology, the University of California, and the National Aeronautics and Space Administration. The observatory was made possible by the generous financial support of the W. M. Keck Foundation. This work was supported by National Science Foundation grant number AST 99-0732 and faculty research funds of the University of California, Santa Cruz.

REFERENCES

Allen, C. W. 1973, Astrophysical Quantities (London: Athlone)
Ashman, K. M., Bird, C. M., & Zepf, S. E. 1994, AJ, 108, 2348
Ashman, K. M., & Zepf, S. E. 1998, Globular Cluster Systems (Cambridge: Cambridge Univ. Press)
Bahcall, J. N., & Tremaine, S. 1981, ApJ, 244, 805
Bertin, E., & Arnouts, S. 1996, A&AS, 117, 393
Binney, J., & Tremaine, S. 1994, Galactic Dynamics (Princeton: Princeton Univ. Press)
Brodie, J. P., & Huchra, J. P. 1990, ApJ, 362, 503
Capaccioli, M., Cappellaro, E., Held, E. V., & Vietri, M. 1993, A&A, 274, 69
Côté, P., Marzke, R. O., & West, M. J. 1998, ApJ, 501, 554
Couture, J., Harris, W. E., & Allwright, J. W. B. 1990, AJ, 73, 671
Da Costa, G. S., & Armandroff, T. E. 1995, AJ, 109, 2533
Dean, J. F., Warren, P. R., & Cousins, A. W. J. 1978, MNRAS, 183, 569
Dekel, A., & Silk, J. 1986, ApJ, 303, 39
de Vaucouleurs, G., de Vaucouleurs, A., Corwin, H. G., Jr., Buta, R., Paturel, G., & Fouque, P. 1991, Third Reference Catalogue of Bright Galaxies (Berlin: Springer)
Durrell, P. R., Harris, W. E., Geisler, D., & Pudritz, R. E. 1996a, AJ, 112, 972
Durrell, P. R., McLaughlin, D. E., Harris, W. E., & Hanes, D. A. 1996b, ApJ, 463, 543
Elson, R. A. W., & Freeman, K. C. 1985, ApJ, 288, 521
Ferguson, H. C., & Binggeli, B. 1994, ARA&A, 6, 67
González, J. J. 1993, Ph.D. thesis, UCO/Lick Observatory
Grillmair, C. J., Ajhar, E. A., Faber, S. M., Baum, W. A., Holtzman, J. A., Lauer, T. R., Lynds, C. R., & O'Neil, E. J., Jr. 1996, AJ, 111, 2293
Heisler, J., Tremaine, S., & Bahcall, J. N. 1985, ApJ, 298, 8
Hilker, M., Infante, L., & Richtler, T. 1999, A&AS, 138, 55
Holtzman, J., Burrows, C. J., Casertano, S., Hester, J. J., Trauger, J. T., Watson, A. M., & Worthey, G. 1995, PASP, 107, 1065
Horne, K. 1986, PASP, 98, 609
Huchra, J., Stauffer, J., & Van Speybroeck, L. 1982, ApJ, 259, L57
Kavelaars, J. J. 1997, Ph.D. thesis, Queen's Univ., Ontario
King, I. 1962, AJ, 67, 471
Kissler-Patig, M., Brodie, J. P., Schroder, L. L., Forbes, D. A., Grillmair, C. J., & Huchra, J. P. 1998a, AJ, 115, 105
Kissler-Patig, M., Forbes, D. A., & Minniti, D. 1998b, MNRAS, 298, 1123
Kissler-Patig, M., Grillmair, C. J., Meylan, G., Brodie, J. P., Minniti, D., & Goudfrooij, P. 1999, AJ, 117, 1206
Kundu, A., & Whitmore, B. C. 1998, AJ, 116, 2841
Kundu, A., Whitmore, B. C., Sparks, W. B., Macchetto, F. D., Zepf, S. E., & Ashman, K. M. 1999, ApJ, 513, 733
Mateo, M. L. 1998, ARA&A, 36, 435
Miller, B. W., Lotz, J. M., Ferguson, H. C., Stiavelli, M., & Whitmore, B. C. 1998, ApJ, 508, L133
Minniti, D., Meylan, G., & Kissler-Patig, M. 1996, A&A, 312, 49
Oke, J. B., et al. 1995, PASP, 107, 375
Peterson, R. C., & Caldwell, N. 1993, AJ, 105, 1411
Pryor, C. & Meylan, G. 1993, in ASP Conf. Ser. 50, Structure and Dynamics of Globular Clusters, ed. S. G. Djorgovski & G. Meylan (San Francisco: ASP), 357
Puzia, T. H., Kissler–Patig, M. K., Brodie, J. P., & Huchra, J. P. 1999, AJ, 118, 2734
Schlegel, D. J., Finkbeiner, D. P., & Davis, M. 1998, ApJ, 500, 525
Searle, L., & Zinn, R. 1978, ApJ, 225, 357
Silverman, B. W. 1986, Density Estimation for Statistics and Data Analysis (Boca Raton: Chapman and Hall/CRC Press)
Trager, S. C., King, I. R., & Djorgovski, S. 1995, AJ, 109, 218
Trager, S. C., Worthey, G., Faber, S. M., Burstein, D., & González, J. J. 1998, ApJS, 116, 1
van de Kamp, P. 1967, Principles of Astrometry (San Francisco: W. H. Freeman)
Worthey, G., Faber, S. M., & González, J. J. 1992, ApJ, 398, 69